The circadian dynamics of the hippocampal transcriptome and proteome is altered in experimental epilepsy

Authors

K. J. Debski[1, 2†], N. Ceglia[3†], A. Ghestem[4†], A. I. Ivanov[4†], G. E. Brancati[4], S. Bröer[5], A. M. Bot[1], J. A. Müller[6], S. Schoch[6], A. Becker[6], W. Löscher[5], M. Guye[7, 8], P. Sassone-Corsi[9], K. Lukasiuk[1], P. Baldi[3], C. Bernard[4]*

Affiliations

[1] Epileptogenesis Lab, Nencki Institute of Experimental Biology of Polish Academy of Sciences, 02-093 Warsaw, Poland.

[2] Bioinformatics Lab, Nencki Institute of Experimental Biology of Polish Academy of Sciences, 02-093 Warsaw, Poland.

[3] Department of Computer Science and Institute for Genomics and Bioinformatics, University of California, Irvine, Irvine, California, USA.

[4] Aix Marseille Univ, INSERM, INS, Inst Neurosci Syst, Marseille, France.

[5] Department of Pharmacology, Toxicology and Pharmacy, University of Veterinary Medicine Hannover, Hannover, Germany.

[6] Department of Neuropathology, University of Bonn Medical Center, Bonn, Germany.

[7] Aix-Marseille Univ, CNRS, CRMBM, Marseille, France

[8] APHM, Hôpital Universitaire Timone, CEMEREM, Marseille, France

[9] Department of Biological Chemistry, University of California-Irvine, Irvine, CA 92697, USA.

[†]Equally contributing authors

*Correspondence to: christophe.bernard@univ-amu.fr

Abstract

Gene and protein expressions display circadian oscillations in numerous body organs. These oscillations can be disrupted in diseases, thus contributing to the disease pathology. Whether the molecular architecture of cortical brain regions oscillates daily and whether these oscillations are modified in brain disorders is less understood. We identified more than 1200 daily oscillating transcripts in the hippocampus of control mice. More hippocampal transcripts (>1600) were oscillating in experimental epilepsy, with only one fourth oscillating in both conditions. Proteomics studies supported these results. Analysis of biological processes predicted time-dependent alterations in energy metabolism in epilepsy, which were verified experimentally. Although aerobic glycolysis activity remained constant from morning to afternoon in controls, it increased in epilepsy. The oxidative pathway was regulated in both conditions but in opposite directions: it increased in control and decreased in epilepsy. We also found a different circadian regulation of the targets of anti-epileptic drugs. Hence, the "control" hippocampus shows a daily remapping of its molecular landscape, which may enable different functioning modes during the night/day cycle. Such circadian regulation of genes and proteins may also occur in other brain regions. Many genes non-oscillating in control animals gained rhythms in experimental epilepsy, suggesting important changes in the circadian regulation of genes and proteins in pathological conditions, hence a different functioning mode. Such alterations may also occur in other neurological disorders. These modifications need to be taken into account not only to study the mechanisms underlying these pathologies, but also to design drug treatments and time their delivery.

Introduction

Circadian rhythms regulate numerous brain functions (e.g. wakefulness, feeding, etc.) with 24-hour oscillations in most species. The core time keeping machinery is the suprachiasmatic nucleus (SCN). The molecular architecture of the SCN undergoes a daily remapping driven by transcriptional and translational feedback loops, thus allowing switching between different functional states (*1, 2*). Several studies suggest the existence of additional (ancillary) clocks in the brain outside the SCN (*3*). Indeed, clock genes, including Per1, Per2, Bmal1, Cry1 and Cry2, exhibit rhythmic expression in a brain region- and gender-dependent manner *(4, 5).* Since these genes are involved in the regulation of transcription/translation of many other genes, brain regions outside the SCN may also undergo a complex daily remapping of their molecular architecture (*6, 7*). In particular, the synaptic transcriptome, proteome and phosphorylome display strong dynamical modifications driven by the sleep-wake cycle (*8, 9*). Such structural alterations may underlie the changes in functional connectivity related to memory networks found during a normal day of wake in control humans (*10*) as well as learning and memory processes *(11-13)*. In the hippocampus, synaptic responses (*14*), long term synaptic plasticity *(15, 16)*, and the memory-associated MAPK pathway (*17*) display circadian rhythmicity. We thus hypothesized that the molecular architecture of the hippocampus is also regulated in the circadian manner. Further, if this hypothesis is verified, we also hypothesized that such circadian regulation would be modified in experimental temporal lobe epilepsy (TLE), as clock genes display different cycling behavior in this condition *(18)*. Since there is a tight relationship between circadian rhythmicity and metabolism (*19, 20*), we used the transcriptomics and proteomics results to predict time- (circadian) and condition- (control versus epilepsy) dependent changes in cell metabolism, which were then tested experimentally. We focused on energy metabolism, because it is a clinically important issue. Patients with epilepsy display altered metabolic activity in specific brain regions; a clinical information that can be used for diagnosis purposes (*21*). Although debated, several

studies report regional and circadian changes in energy metabolism in healthy humans, as measured by PET, functional MRI, MR spectroscopy, and glucose sensing in the cerebrospinal fluid (*10, 22-26*). Circadian changes in metabolism may be altered in epilepsy, as already demonstrated in patients with depression as compared to healthy controls (*27*). We thus tested the hypothesis that energy metabolism is altered in experimental epilepsy in a time of the day-dependent manner, using the database to predict which metabolic pathways may be specifically altered. As a final readout of the database, we assessed whether the molecular targets of some antiepileptic drugs display circadian rhythmicity in experimental epilepsy, a key issue to consider for the proper timing of drug delivery *(28, 29)*.

Results

Circadian regulation of genes and proteins in the mouse hippocampus

Animals were kept under a regular light/dark cycle, and brain samples were collected every 4 hours, to obtain 6 time points. Since the distribution of transcripts is heterogeneous along the septo-temporal axis of the hippocampus *(22)*, we focused on its ventral part *(23)*, which is most epileptogenic in human TLE and experimental models *(24)*. Using Affymetrix microarrays and the Jonckheere-Terpstra-Kendall (JTK) algorithm (*30*), we identified 1256 transcripts oscillating in the ventral hippocampus of control mice (Fig. 1A and Supplementary Table 1). Hence, 10% of hippocampal genes are regulated in a circadian manner, as compared to 19% in the SCN *(4)* and 6% in the forebrain (*9*). Data from postmortem human hippocampus suggests that less genes (n=659) are oscillating *(7)*. Comparison with the latter study is difficult because investigating circadian rhythms requires a strict control of circadian conditions (e.g. no light exposure during the night), which could not be achieved in the human study. Our results are also consistent with the diurnal regulation of genes in non-human primates (*31*).

Using one-way ANOVA and a false discovery rate <0.05 followed by cluster analysis and functional analysis with DAVID – The Database for Annotation, Visualization and Integrated

Discovery (https://david.ncifcrf.gov/), we found 486 transcripts differentially expressed, which could be identified based on biological functions (Fig. 1A-C). When compared to subcortical structures (Table 1), we found a clear overlap of core clock genes involved in transcriptional and translational feedback loops in the SCN across all investigated brain regions (highlighted in green in Table 1). Oscillating core clock genes in the hippocampus included Per1-3, Cry1, Arnt1, Nr1d1-2, and Dbp (Fig. 2A-B, Table 1). Transcriptome analysis was confirmed with qPCR on selected genes, including some core clock genes (fig. S1). Interestingly, a large set of oscillating genes was specific to the hippocampus (Table 1), demonstrating that circadian rhythmicity of genes is brain region-dependent.

The analysis of the heatmaps (fig. S2) revealed that gene oscillations were distributed with either a very low or very high oscillation amplitude in control mice (Fig. 3A). The majority of genes with high amplitude oscillations were phase advanced in comparison to the rest of the oscillatory transcripts (Fig. 3A).

Proteomic data enabled the analysis of 1,500 peptides. We found 170 peptides oscillating in controls (table S2), i.e. the same percentage (11%) as for gene transcripts. Nine proteins were oscillating in both proteomic and transcriptome datasets. The rather small overlap between the transcriptome and proteome datasets is due to the following reasons. Numerous genes were below detection levels and did not have correspondence in the proteome dataset (for example, HDAC1 and HDAC2 are not represented in the transcriptome dataset). Conversely, proteins were identified with at least two peptides (with at least one unique to the protein). We applied relatively stringent criteria to control for false positives: we used the “posterior error probability” for each spectrum match (peptide identification) in order to filter for 1% false-discovery-rate (FDR) on spectrum-match level. We were therefore quite conservative to avoid false-positives and thus lost some sensitivity. RNA micro arrays are targeting pre-defined transcripts while the mode of measurement for proteome analyses is untargeted and suffers from stochastic sampling. In

addition, proteome favors the most abundant proteins not the most biologically interesting ones. Despite this, we found the same percentage of oscillating proteins as for gene transcripts.

Together these results demonstrate that 10% of the gene/protein map in the hippocampus of control mice undergoes a continuous remapping during the night/day cycle. We then performed the same analysis in age-matched TLE mice in order to determine whether such circadian regulation was maintained in pathological conditions.

Altered circadian regulation of genes and proteins in experimental TLE

In experimental TLE (pilocarpine model), the number of oscillating transcripts was increased by 30% as compared to control (1650 versus 1256, Fig. 1A and table S3). Remarkably, only 29% of the oscillating transcripts were common to both control and TLE conditions, demonstrating a large modification of the daily remapping of hippocampal genes. Cluster analysis of differentially expressed genes in control or TLE animals clearly separated the different groups by time and function (Fig. 1B). The core clock genes all gained in oscillation amplitudes in TLE as compared to control (Fig. 2A-B). Many important circadian-related genes gained oscillatory activity in TLE, from which we highlighted Bhlhe40 and Bhlhe41 (Fig. 2B and 3B). Bhlhe40 and Bhlhe41 have been shown to be components of a separate negative feedback loop with Clock/Bmal1. Given that Bhlhe40 and Bhlhe41 have binding sites identified upstream of Per1 and Per2 from MotifMap (FDR – false discovery rate < 0.25, BBLS – Bayesian Branch Length Score > 1.0), increased oscillations of Bhlhe40 and Bhlhe41 may play a key role in the larger recruitment of oscillating transcripts in TLE *(32, 33)*. It will be important to understand the causes and consequences of increased oscillatory activity of core clock genes in TLE.

The database we provide may help addressing such issues to propose working hypotheses. As an example, we noticed that Runx1, a DNA binding regulator, gained statistical significance in TLE (Fig. 2B and 3B). Several studies report that Runx1 regulates core circadian transcription

factors *(34, 35)*. Among these, Per1 and Per3 contain statistically significant transcription factor binding sites in the promoter region for Runx1 *(32)*. Additionally, rhythmic expression of Runx1 in TLE peaks ~4 hours before Per1 and Per2. Since the mean delay between the time when a circadian transcript reaches its peak of expression and the time for the subsequent protein to reach its peak of expression is ~4 hours *(36)*, Runx1 may be involved in the amplification of oscillation in the TLE. In addition, Runx1 has protein-protein interaction with two key histone deacetylases, Hdac1 and Hdac2. In keeping with this, proteomics revealed oscillatory activity for Hdac1 and Hdac2 in TLE (table S4). Finally, Hdac8 also gained oscillatory activity in TLE. Together, these results suggest that the gain in oscillatory activity of key circadian-related genes in TLE may be driven by regulatory genes starting to oscillate in TLE, such as Runx1. This hypothesis remains to be tested, and the mechanisms underlying the recruitment of Runx1 in TLE warrants further investigation.

In the experimental TLE condition, 705 of the 782 oscillating transcripts showed a greater than 10% increase in amplitude over the average amplitude found in the control condition. For those oscillating transcripts with an increased amplitude, we find proportionally more phase advanced (defined as a greater than 10% forward shift in phase over the control condition) oscillating transcripts in the TLE alone condition (Fig. 3B and fig. S2).

As for transcripts, the number of oscillating peptides was increased by 40% in TLE as compared to control (237 versus 170 peptides, Fig. 2C and table S4), with only 5% common to both experimental groups.

We conclude that there is a drastic change in the daily dynamics of genes and proteins in experimental TLE as compared to control. Not only the set of oscillating genes is modified, but also the amplitude of the oscillation and the phase (i.e. at what time during the night and day cycle).

Functional significance

The enriched terms reported from DAVID bioinformatics for oscillating genes found in control condition alone, epileptic condition alone, and oscillating in both conditions for three different p-values are listed in tables S5-S13. The Gene Set Enrichment Analysis (GSEA) reported many biological pathways, including those linked to metabolism, showing circadian regulation in control and TLE, and specific alterations in TLE as revealed by KEGG – Kyoto Encyclopedia of Genes and Genomes (https://www.genome.jp/kegg/) – pathways gene sets, Gene Ontology biological process, Gene Ontology metabolic function and REACTOME (a free, open-source, curated and peer-reviewed pathway database; https://reactome.org/) (fig S3-S14, table S14-S25).

In order to show how the resource we provide can be used to predict/test functional consequences, we focus on the main energy metabolism pathways, such as aerobic glycolysis and oxidative phosphorylation which are known to be altered in patients with TLE and experimental TLE (*37-41*). In order to compare the activity of genes involved in energy metabolism, we quantified gene set differential expression including gene-gene correlations (*42*). Gene sets were selected from Molecular Signatures Database v7.0 (MsigDB, (*43, 44*)), using keywords: "LACTATE.*", "GLYCOLYSIS.*", "GLUCOSE.*", "PENTOSE.*", "CITRIC.*", "GLYCOGEN.*", "PYRUVATE.*", "CIRCADIAN.*", "OXIDATIVE_PHOSPHORYLATION.*", "NEURON_CELLULAR_HOMEO.*", "NEURON_DEATH.*". We compared the selected gene set activity at each time point for control and epileptic animals (Fig. 4A). No gene sets displayed constant differences in their activity at all time points suggesting that circadian regulation in TLE is not paralleled with that of control. The majority of gene sets involved the energy metabolism are less active in TLE at least at one time point and their activity is never higher than that in control mice even at ZT9 when seizures have

the highest probability to occur (Fig. 5A). Interestingly, the activity of gene sets related to glucose uptake and transport, as well as to glycolysis regulation are downregulated in TLE at ZT1 only. At all other time points, the activity is similar to control (highlighted in green in Fig. 4A). We thus predicted a lower glucose utilization at the beginning of the light phase (ZT1-ZT4) in TLE, followed by a normalization to control levels later on. The heat map led to a second prediction: oxidative phosphorylation should be similar in control and TLE during the ZT1-5 time interval but should decrease in TLE at ZT9 (Fig. 4A, light blue arrow). In order to test both predictions, we evaluated energy metabolism activity *ex vivo* in ventral hippocampal slices using two distinct methods, NAD(P)H imaging and glucose/lactate sensing. Hippocampal slices were obtained at ZT3 and at ZT8. Schaffer collateral stimulation produced characteristic transient changes in NAD(P)H fluorescence intensity in the stratum radiatum of the CA1 region: the initial 'dip' was followed by the 'overshoot' component, reflecting enhanced oxidation and reduction of the pyridine nucleotide, respectively (Fig. 4Ba, Bb). The overshoot amplitude is related to the intensity of cytosolic glycolysis in both astrocytes and neurons while the initial "dip" is associated with mitochondrial oxidative metabolism (*45*). In slices prepared at ZT3 (Fig. 4Ba), the NAD(P)H transient overshoot was significantly smaller in TLE than in control mice (mean amplitude: 1.3±0.17% n=9 vs 3.5±0.5%, n=10, $p<0.01$) suggesting reduced activity of cytosolic glycolysis in TLE as compared to control. However, in slices prepared later, there was no difference in the overshoots (TLE: 4.1±0.4%, n=6, control: 4.6±0.9%, n=6, p=0.3) indicating that glycolytic activity in TLE reached control levels (Fig. 4Bb). This result validates the first prediction. The initial 'dip' of NAD(P)H transient was similar in control slices at both time points (ZT3: -1.9±0.2% vs ZT8: -1.7±0,4, p=0.7, n=6), but was decreased in TLE at ZT8 as compared to ZT3 (-0.6±0.1% vs -1.3±0.2% n=6, $p<0.01$; Fig. 4Bb gray arrowheads), indicating a reduction in the intensity of oxidative phosphorylation, verifying the second prediction.

In the next set of experiments we used the same experimental condition and stimulation protocol but measured extracellular glucose or lactate using enzymatic sensors inserted in the stratum radiatum of CA1. Schaffer collateral stimulation triggered a decrease in extracellular glucose indicating its consumption by cells (Fig. 4Bc, Bd), leading to an increase of L-lactate in the extracellular space (Fig. 4Be, Bf). This indicates that glucose was metabolized to pyruvate that was then partially reduced to L-lactate and finally released. The remaining pyruvate entered mitochondria to fuel oxidative energy metabolism. At ZT3, glucose consumption was lower in TLE than in control (maximal concentration change: 0.13±0.03mM vs 0.52 ± 0.14mM, $p<0.01$, n=9, Fig. 4Bc), paralleling a smaller amount of released L-lactate (maximal concentration change: 0.04±0.01mM vs 0.19 ± 0.05mM, $p<0.01$, n=7, Fig. 4Be). Thus, aerobic glycolysis is lower in TLE than in control at ZT3. At ZT8, glucose consumption was increased in both groups (Fig. 4Bd) remaining larger in control as compared to TLE (1.00 ±0.4 mM vs 0.41± 0.08 mM, $p<0.05$, n=5). Lactate release was increased at ZT8 as compared to ZT3 in TLE (0.12 ± 0.01mM, n=6 vs 0.04±0.01mM, n=7, $p<0.01$), while in control it decreased at ZT8 as compared to ZT3 (0.11 ± 0.01mM, n=6 vs 0.19±0.05mM, n=7, p=0.06). Together, these results show major time-dependent differences in energy metabolism between TLE and control animals. In TLE, glucose consumption increased together with lactate production, demonstrating enhanced aerobic glycolysis. In controls, lactate release remained unchanged although glucose consumption increased. This means that the intensity of aerobic glycolysis, producing lactate, remained constant while oxidative metabolism was enhanced via the consumption of additional glucose. Finally, we noted that lactate was decreasing at the beginning of synaptic stimulation in controls at ZT8 (Fig. 4Bf, gray arrowhead), indicating either decreased lactate production, because more pyruvate entered into the mitochondria, or lactate uptake and its oxidation to pyruvate. Both scenarios support enhanced oxidative metabolism in controls at ZT8. We conclude that one of the functional consequences of the altered circadian regulation in TLE is a differential, time-dependent, recruitment of metabolic pathways. In control conditions, only oxidative metabolism

intensity is changing (increasing) between ZT3 to ZT8, while aerobic glycolysis remains constant. In experimental TLE, both oxidative metabolism and aerobic glycolysis are regulated in a time-dependent manner in opposite directions: the oxidative pathway is decreasing and the aerobic electrolysis is increasing between ZT3 to ZT8.

The circadian rhythmicity can also be appreciated at the system level. Seizures are regulated in a circadian manner in human and experimental mesial TLE (*46*), a result we confirmed in our mouse model (Fig. 5A). One explanation could be that the daily remapping of the molecular landscape brings neuronal networks close to seizure threshold at specific time points *(47)*. In line with this scenario, we found different seizure susceptibility at different time points between control and TLE animals (fig. S15). This further exemplifies the fact that control and TLE animals operate under different functional states.

Consequences for antiepileptic drug targets and chronotherapy

Another possible use of the resource we provide is for drug target design and chronotherapy. Many common drugs (e.g. for gastritis, chronic pain, asthma, and rheumatoid arthritis) target products of genes characterized by circadian rhythmicity (*29*). We obtained information on drugs and genes from DrugBank database version 5.0.6 (a unique bioinformatics and cheminformatics resource that combines detailed drug data with comprehensive drug target information; https://www.drugbank.ca/) *(48)*, which contains information about 8283 drugs including 62 drugs that exert antiepileptic and anticonvulsant effects. In the database, we found mammalian genes encoding 2230 drug targets, 35 drug carriers, 238 drug enzymes and 130 drug transporters. For the 62 antiepileptic/anticonvulsant drugs, we found genes encoding 102 drug targets, 1 drug carrier, 32 drug enzymes and 18 drug transporters.

Among the genes that oscillate in control and TLE animals (JTK_CYCLE – an efficient nonparametric algorithm for detecting rhythmic components in genome-scale data sets – adjusted

$p < 0.05$), we found 24 and 71 drug targets, 2 and 2 drug carriers, 2 and 7 drug enzymes, and 2 and 9 drug transporters, respectively (Table 2). There was little overlap between control and experimental TLE datasets, further highlighting the necessity to take into account the reorganization of gene variations in experimental TLE. We obtained similar conclusions when looking at genes which expression changes (one-way ANOVA, FDR < 0.05) in at least one time point in control and TLE animals. We found 20 and 62 drug targets, 2 and 0 drug carriers, 2 and 11 drug enzymes, and 2 and 7 drug transporters, respectively (Table 2). Table 3 provides examples of oscillating and differentially expressed gene products controlled by antiepileptic and anticonvulsant drugs. Finally, new classes of antiepileptic drugs targeting AMPA and NMDA receptors are being developed (*49*). Remarkably, many of the corresponding genes of AMPA and NMDA subunits present in the database showed different expression patterns at specific time points in TLE as compared to control (Fig. 5B, C).

Together these results suggest that the effects of antiepileptic and anticonvulsant drugs may be time-dependent. It is important to stress that drug efficacy testing must be performed in experimental models of chronic epilepsy as the time-dependent regulation of the drug targets are different in TLE and control conditions. The resource we provide can be used to assess such factor. Whether results obtained in this rodent model can be translated to humans remains to be determined.

Discussion

We conclude that hippocampal networks undergo a complex daily remapping at the gene and protein level. The number of oscillating genes and proteins is likely to be an underestimate as hippocampal samples were collected every four hours. The remapping may drive hippocampal networks into different functioning modes in a circadian-dependent manner to optimize information processing at specific time points. For example, the remapping may contribute to the

circadian regulation of theta oscillations and place cell firing in the hippocampus *(50, 51)*, or, if a remapping also occurs in the cortex, to the circadian regulation of cortical excitability in humans *(52)*. Such oscillations could be a downstream consequence of those occurring in the SCN, and the daily activation of various hormonal and neuromodulator pathways *(13)*. Alternatively, the clock could be intrinsic since some hippocampal genes continue to oscillate *ex vivo (53)*. Yet, the daily molecular remapping is important to consider for understanding hippocampal function. For example, it may influence memory circuit variability during wake as demonstrated by resting-state fMRI (*10*). Since multiple other damped (secondary) circadian oscillators exist in the brain, each with specific phase properties (*54*), it is likely that a remapping also exists in other brain regions, each with a specific set of regulated genes and proteins. In addition, a similar resource should be provided for other hippocampal regions (like the dorsal hippocampus), since the molecular architecture of the hippocampus is not homogenous along its septo-temporal axis *(55)*.

One major limitation of our approach is to lump all cell types from the different hippocampal subfields. Future studies should focus on cell-type specific analysis *(56)*, a complex endeavor since it requires instantaneous "freezing" of cells and networks to stop the cycling process at specific times during the night and day cycle. Likewise, we could not account for the cell loss that is present in TLE models, which may shift the balance between cell types. In addition to mixing different cell types, we could not distinguish between cell compartments (in neurons, the expression of proteins is different in the dendrites, soma, axon). Although mixing samples from different forebrain regions, the synaptic transcriptome, proteome and phosphorylome display strong dynamical modifications driven by the sleep-wake cycle for many more genes and proteins than in the present study (*8, 9*). Mixing cell types and cell compartments may produce noise in the data, and the current 10% value for ventral hippocampus genes may be an underestimate.

In epilepsy, we report a large reprogramming of the cycling behavior, with the possible involvement of epigenetic mechanisms (*57, 58*). It is not yet possible to determine whether this is

a cause or consequence of seizures, altered sleep/wake cycles, or just a homeostatic mechanism. In addition, since mice were kept in colonies to reduce social isolation-induced stress (*59*), it was not possible to assess when each of them had a spontaneous seizure. Although we are not aware of any study reporting a change in gene/protein expression following a spontaneous seizure in a chronic model of TLE, we cannot rule out such possibility.

Based on the database, we predicted and verified experimentally a drastic change in time-dependent regulation in metabolic activity in experimental TLE as compared to control. Whether such alteration in energy production is a compensatory mechanism or is involved in seizure genesis (or co-morbidities such as cognitive deficits and depression) remains to be determined. If our results can be translated to patients, it means that time-of-the-day becomes a critical factor to consider when performing brain imaging to assess metabolic activity in patients. The fact that circadian changes in metabolism are different between healthy individuals and patients with depression (*27*) supports the proposal that the dynamics of brain metabolism are different in pathological conditions as compared to control; an essential parameter to consider for mechanistic studies.

The key result is that the hippocampus uses a different functional regime in TLE as compared to control. This makes comparing genes and proteins beteen control and TLE tissues very difficult, as down or up-regulation could just sign different oscillating properties in both conditions (e.g. a phase shift). Said differently, a given protein may be downregulated at time t in TLE as compared to control, but upregulated at time $t+\Delta t$, which renders the functional interpretation of the observation more complicated. Based on this novel information, it will be now important to indicate the circadian time a given animal was used in any experimental condition, and to take into consideration a possible altered gene/protein rhythmicity when studying neurological disorders. It is possible that such altered circadian rhythmicity may occur in most (if not all) neurological disorders (*60*). This argument is even more crucial for

chronotherapeutics (*28*), highlighting the necessity to take into account the fact that the level of proteins targeted by drugs may not only display circadian rhythmicity but also a rhythmicity that is different between control and pathological conditions.

Materials and Methods

Animals

All experiments were performed on FVB adult male mice following INSERM procedures. All animals had the same age (less than one-week difference), and tissue collection was performed when animals were 14 weeks-old. Twenty-four control and twenty-four TLE mice were used for transcriptomics and proteomics. They were kept in a special in-house animal facility with a strict control of light and temperature conditions (beginning of the light phase at 7:30 and beginning of the night phase at 19:30). A red light, which does not disrupt circadian rhythmicity, was present during the night phase to allow researchers to manipulate the animals. During the night phase, no external light could enter the room when opening the door. Mice were housed in groups of four to five to enable social interaction. Cages had enriched environment. Throughout the experimental procedure, the same researcher took care of the animals at the same time of the day to limit external stressful factors. Animals were anesthetized with isoflurane in the animal facility and four of them killed every four hours (six time points).

The brain was quickly extracted and the hippocampus removed in modified ice cold ACSF. Right (for transcriptome analysis) and left (for proteomics) extracted hippocampi were separated into two halves, i.e. ventral and dorsal parts, and quickly frozen. Only the ventral parts were used here. The average time between decapitation and sample freezing was 90s per mice to limit any degradation of gene products and proteins. All tissue collection was performed during a single 24h period. The collection of the hippocampal tissue from the four mice per time window was performed in less than 10 minutes.

Model of epilepsy

Adult FVB mice were injected with methylscopolamine (1 mg/kg i.p.) 30 min before the pilocarpine injections. Pilocarpine was repeatedly injected (100 mg/kg i.p.), every twenty minutes, until status epilepticus (SE) was observed. After 90 min of SE, we injected diazepam (10 mg/kg i.p.) to stop SE. All mice then received 0.5 ml NaCl (0.9%) subcutaneously, and again in the evening. During the following days, if required, mice were fed with a syringe.

24/7 EEG monitoring

Ten mice were implanted with a telemetry probe (ETA F10, (Data Science International [DSI], St Paul, MN) for EEG analysis only (the brain was not harvested for transcriptome or connectome analysis). The stereotaxic surgery was performed under ketamine (100mg/kg) / xylazine (10mg/kg) anesthesia. Lidocaine was used locally. Temperature, heart rate, and breathing rate were continuously monitored during the surgical procedure using MouseOx®Plus monitor (Starr Life Sciences Corp Oakmont, PA, USA). A recording skull screw was secured above the hippocampal CA1 region (-1.8mm posterior, +1.8mm lateral), and a reference skull screw was secured above the cerebellum. The leads of the DSI telemetry probe (Data Science International, St Paul, MN) were wrapped around the recording and reference screws, and screws were all encased in dental cement. The probe body containing the battery was placed subcutaneously in the back of the mice. Animals were allowed 7 days postsurgical recovery before any further experimental procedures were conducted. Electroencephalographic (EEG) recordings were performed continuously until the end of the experimental protocol. Seizures were automatically detected with DSI software (adjusting for frequency and amplitude) using low detection values. This led to numerous false positives (mostly movement artifacts), which were manually removed after double-checking by a trained technician and clinical epileptologist. Complete EEG recordings were fully visually inspected. No false negatives were detected (i.e., the semi-automated procedure insured the detection of all seizures).

All pilocarpine-treated mice developed spontaneous seizures.

Animal care and handling

We kept 6 mice (control or epileptic) per cage, with enriched environment. We found that keeping epileptic mice together (as opposed to one mouse per cage) dramatically changed their behavior. They recovered faster from status epilepticus. They could be easily handled, denoting a lack of stress. When epileptic mice are housed in individual cages, they are extremely nervous and it is very difficult to handle them. Here, we removed a confounding stress factor linked to the lack of social interaction, as reported in rats *(47)*.

Seizure threshold tests with pentylenetetrazole (PTZ)

Seizure threshold was determined in individual male FVB mice by the timed intravenous pentylenetetrazole (PTZ) test as described previously *(48)*, in a total of 57 naive and 55 epileptic mice. Epilepsy was induced by pilocarpine *(49)* and seizure thresholds were determined 7-9 weeks after SE, when all mice had developed epilepsy. Groups of 8–20 mice were used per threshold determination. PTZ infusion was stopped at the first seizure, and seizure threshold was calculated in mg PTZ per kg body weight based on the infusion time needed to induce this seizure endpoint *(48)*. PTZ thresholds were determined every 4 hours during the light and dark phase. The maximum number of threshold determinations was limited to 3 per animal with 7 days in between (repeated seizure threshold tests do not alter the threshold if an interval of at least 48 h lies within the determinations) *(48, 50, 51)*. Additionally, we performed two PTZ seizure threshold determinations at the same time-point (ZT4:30) to compare PTZ thresholds at the beginning and at the end of the experiment, demonstrating the reproducibility of the method. Data were analyzed by using the Prism5 software (GraphPad, La Jolla, CA, USA). Thresholds of control and SE animals were analyzed separately using one-way analysis of variance (ANOVA) and Bonferroni post-hoc tests and combined by using a two-way ANOVA with Student's *t*-tests as post hoc analysis. All tests were used two-sided; a $P < 0.05$ was considered significant.

RNA isolation and microarray hybridization

The isolation of total RNA was performed using the miRNeasy Mini kit (QIAGEN, # 217004) according to the manufacturer's instructions. The sample quality was determined using a NanoDrop 2000 spectrophotometer (Thermo, Fisher Scientific) and Agilent 2100 Bioanalyzer. GeneChip® Mouse Gene 2.1 ST arrays (Affymetrix, Santa Clara, CA, # 902120) were used for mRNA profiling. One hundred nanograms of total mRNA was used for cDNA synthesis using the Ambion WT Expression Kit (Life Technologies, # 4411974). Hybridization, washing and scanning were conducted according to Affymetrix guidelines for the GeneAtlas™ instrument.

Quantitative PCR

Reverse transcription for individual qPCRs was carried out using 250 ng of total RNA and the High-Capacity Reverse Transcription Kit (# 4368814, Life Technologies) according to the manufacturer's instruction. Quantitative PCRs were run on the ABI 79OOHT Fast Real-Time PCR instrument (Applied Biosystems). Gene expression analysis was conducted using a relative standard curve method with glyceraldehyde-3-phosphate dehydrogenase (Gapdh) to normalise the expression levels of target genes. All reactions were performed in triplicates.

Bioinformatic analysis

Analysis of microarrays was performed using R/Bioconductor (R Core Team, 2014; www.bioconductor.org). All microarrays were normalized with the Robust Multi-array Average (RMA) algorithm using oligo package (version 1.28.3)*(52)*. Background value of intensity of probes was defined as median value of the intensity of antigenomic probes. The intensity of genomic probes below the background intensity was corrected to this background value. Probes with intensity greater than background value in less than four samples were removed from analysis. Only probes that corresponded to a single gene were selected for further analysis. JTK_Cycle and BIO_CYCLE were used to identify oscillating genes at three p-value thresholds*(25)*. Gene lists for transcripts oscillating at each p-value in the control condition alone,

the TLE condition alone, or both conditions were identified for further analysis. Cyber-T was used to identify differentially expressed transcripts between control and TLE conditions in each time point *(53)*. Cyber-T p-values found for each time point for core clock genes are reported (Fig. 2A). Proteomic data for both control and TLE conditions was also analyzed by JTK_Cycle to identify rhythmic proteins. All transcriptome data is available for search on Circadiomics along with JTK_Cycle and BIO_CYCLE results *(54)*.

Genes, which expression level differed between time points according to one-way ANOVA analysis performed separately for control and epileptic animals are presented on the heatmap (Fig. 1B). Differences were considered as significant for adjusted p-value < 0.05 (FDR – Benjamini & Hochberg (BH) correction). Genes were ordered by clustering complete-linkage method together with Pearson correlation distance measure. Nine gene clusters highlighted on the heatmap were obtained by cutting dendrogram the selected level of the dendrogram. Functional analysis for Biological Function Go Terms was performed using MF FAT Chart option with default settings in DAVID with (http://david.abcc.ncifcrf.gov; *(55, 56)*). The Gene Set Enrichment Analysis (GSEA) *(57)* (http://software.broadinstitute.org/gsea/index.jsp) was performed based on gene sets obtained from Molecular Signatures Database v5.0 (mSigDB) (http://software.broadinstitute.org/gsea/msigdb/index.jsp). For GSEA, a ranking based score - log10(pvalue) * sign(fold change) was used. P values and fold changes were obtained from comparisons with t-test between two consecutive time points in control and TLE animals separately (fig. S3-S8) or between control and TLE animals at each time point (fig. S9-S14). The GSEA was performed with weighted enrichment statistic, meandiv normalization mode, max probe collapsing mode and with min/max size restriction (10/1000). Gene sets were considered as down- or up- regulated if nominal p value < 0.05 and FDR < 0.25. Transcription factor binding sites overrepresented in promoters within clusters were detected with gProfiler (http://biit.cs.ut.ee/gprofiler/; *(58, 59)*) with custom background defined as genes detected in the experiment to reveal the functional and regulatory groups presented in the data.

Further transcription factor binding site enrichment analysis was performed using MotifMap *(26, 28)* and CHiP-seq datasets provided by UCSC Encode project *(60)*. Transcription factor binding sites identified by MotifMap were found both 10 KB upstream and 2 KB downstream of transcription start sites (TSS) for all genes in each of the differentially expressed gene lists for all pair-wise comparisons. The motifs identified were found with a BBLS conservation score of greater than or equal to 1.0 and an FDR of less than 0.25. CHiP-seq datasets were used to locate experimentally identified binding site locations within the same interval around the TSS for differentially expressed genes. Only the 90th percentile of CHiP-seq peaks were used from each dataset provided by UCSC Encode. A Fisher's exact test was performed separately using the full background list of motifs from MotifMap and all target genes from the CHiP-seq datasets to compute the statistical likelihood of over representation in promotor regions.

Proteomics

Protein extraction. All steps of the protein extraction were performed on ice or at 4°C. Isolated hippocampal tissue was homogenized in lysis buffer containing 20 mM triethylammonium bicarbonate (TEAB, Fluka), 5 % sodium deoxycholate (SDC, Sigma-Aldrich) and 1 tablet of protease inhibitor (Roche). Homogenates were boiled for 3 minutes and subsequently sonicated three times for 10 s, each time paused for 30 s.

Samples were centrifuged to pellet tissue debris and the protein concentration in the supernatant was measured with a BCA protein assay (Pierce) using bovine serum albumin as standard.

Protein Digestion. Dithiotreitol (DTT) was added to 200 µg of the global protein fraction up to a final concentration of 20 mM DTT in the solution. Samples were incubated for 20 min at 55°C and then centrifuged for 1 minute at 10000xg (20 °C). The supernatant was transferred to filter devices (10kDa MWCO, VWR) and filled up with digestion buffer (DB) containing 20 mM TEAB and 0.5 % SDC. Next, the samples were centrifuged for 10 minutes at 10000xg (20 °C), the flow-through was discarded and 100 µl of 40 mM Indoacetamide (IAA) in DB was added to

the filter devices followed by a 20 min incubation at room temperature in darkness. Afterwards samples were washed twice with DB and trypsin solved in DB was added to yield a protein to trypsin ratio of 100:1. Samples were incubated over night at 37°C. Filter devices were centrifuged for 20 minutes at 10000xg (20 °C) and the flow-through was collected. Residual peptides were removed by another centrifugation step with DB. The flow-throughs of one sample were combined and first an equal volume of ethyl acetate and subsequently trifluoreoacetic acid (TFA, final concentration 0.5%) was added. The solution was mixed and centrifuged for 2 minutes at 14000xg (20 °C). The upper layer was discarded and 250 µl of acetate ethyl was added, followed by centrifugation. The upper layer was discarded again and the aqueous phase was collected for further procession.

Isobaric labeling and peptide fractionation. Peptides were vacuum concentrated and labeled with amine-reactive, 6-plex tandem mass tag reagents (Thermo Fisher Scientific, Bremen, Germany) according to manufacturer's instructions. The labeling reaction was quenched by addition of 5% hydroxylamine. Labeled peptides were pooled and desalted on Oasis HLB cartridges (Waters GmbH, Eschborn, Germany). Eluates containing 70% acetonitrile, 0.1% formic acid (FA) were dried and fractionated to 24 fractions by isoelectric point with an Offgel fractionator according to manufacturer's recommendations (Agilent Technologies, Waldbronn, Germany). Peptide fractions were dried and stored at -20 °C.

LC-MS analysis. Peptides were dissolved in 8 µl 0.1% trifluoroacetic acid. 1.5 µl were injected onto a C18 trap column (20 mm length, 100 µm inner diameter) coupled to a C18 analytical column (200 mm length, 75 µm inner diameter), made in house with 1.9 µm ReproSil-Pur 120 C18-AQ particles (Dr. Maisch, Ammerbuch, Germany). Solvent A was 0.1% formic acid. Peptides were separated during a linear gradient from 4% to 40% solvent B (90% ACN, 0.1%

formic acid) within 90 min. The nanoHPLC was coupled online to an LTQ Orbitrap Velos mass spectrometer (Thermo Fisher Scientific). Peptide ions between 330 and 1800 m/z were scanned in the Orbitrap detector with a resolution of 30,000 (maximum fill time 400 ms, AGC target 10^6, lock mass 371.0318 Da). The 20 most intense precursor ions (threshold intensity 5000) were subjected to higher energy collision induced dissociation (HCD) and fragments also analyzed in the Orbitrap. Fragmented peptide ions were excluded from repeat analysis for 15 s. Raw data processing and analyses of database searches were performed with Proteome Discoverer software 1.4.1.12 (Thermo Fisher Scientific). Peptide identification was done with an in house Mascot server version 2.4.1 (Matrix Science Ltd, London, UK). MS2 data (including a-series ions) were searched against mouse sequences from SwissProt (release 2014_01). Precursor Ion m/z tolerance was 10 ppm, fragment ion tolerance 20 mmu. Tryptic peptides were searched with up to two missed cleavages. Low scoring spectrum matches were searched again with semitryptic specificity with up to one missed cleavage. Oxidation (Met), acetylation (protein N-terminus), and TMTsixplex (on Lys and N-terminus) were set as dynamic modifications, carbamidomethylation (Cys), was set as static modification. Mascot results from searches against SwissProt were sent to the percolator algorithm *(61)* version 2.04 as implemented in Proteome Discoverer. Only proteins with two peptides (maximum FDR 1%) were considered identified.

In vitro experiments

Tissue slice preparation. Mice were anaesthetized with isoflurane and decapitated at ZT4 or ZT8. The brain was rapidly removed from the skull and placed in the ice-cold ACSF as above. The ACSF solution consisted of (in mmol/L): NaCl 126, KCl 3.50, NaH_2PO_4 1.25, $NaHCO_3$ 25, $CaCl_2$ 2.00, $MgCl_2$ 1.30, and dextrose 5, pH 7.4. ACSF was aerated with 95% O_2/5% CO_2 gas mixture. Slices of ventral hippocampus (350 µm) were cut as described *(62)*, using a tissue slicer (Leica VT 1200s, Leica Microsystem, Germany). The ice-cold (< 6°C) cutting solution consisted of (in mmol/L): K-gluconate 140, HEPES 10, Na-gluconate 15, EGTA 0.2, NaCl 4, pH adjusted to 7.2 with KOH. Slices were then immediately transferred to a multi-section, dual-side perfusion

holding chamber with constantly circulating ACSF and allowed to recover for 2h at room temperature (22°C-24°C). Slices were then transferred to a recording chamber continuously superfused with ACSF (flow rate 7ml/min, warmed at 30–31°C) with access to both slice sides.

Synaptic stimulation and field potential recordings. Schaffer collaterals were stimulated using a DS2A isolated stimulator (Digitimer Ltd, UK) with a bipolar metal electrode. Stimulus current was adjusted using single pulses (100-250 µA, 200µs, 0.15 Hz) to induce a local field potential (LFP) of about 60% of maximal amplitude. LFPs were recorded using glass microelectrodes filled with ASCF, placed in stratum pyramidale and connected to an EXT-02F/2 amplifier (NPI Electronic GmbH, Germany). Synaptic stimulation consisting of a stimulus train (200µs pulses) at 10 Hz lasting 30s was used to trigger metabolic response.

NAD(P)H fluorescence imaging and extracellular glucose/lactate measurement. NADPH and NADH have similar optical properties, therefore it is expected that NADPH may contribute to the total autofluorescence signal. Because the cellular $NADP^+$/ NADPH pool is about one order of magnitude lower than the NAD/NADH pool, in the present study we assume that short-term variations of experimentally detected fluorescent changes responses account for variations in NADH (see discussion in *(63)*). Here, for the fluorescent signal we use the term NAD(P)H. Changes in NAD(P)H fluorescence in hippocampal slices were monitored using a 290–370 nm excitation filter and a 420 nm long-pass filter for the emission (Omega Optical, Brattleboro, VT). The light source was the pE-2 illuminator (CoolLed, UK) equipped with 365 nm LED. Slices were epi-illuminated and imaged through a Nikon upright microscope (FN1, Eclipse) with 4x/0.10 Nikon Plan objective. Images were acquired using a 16-bit Pixelfly CCD camera (PCO AG, Germany). Because of a low level of fluorescence emission, NAD(P)H images were acquired every 600-800 ms as 4x4 binned images (effective spatial resolution of 348x260 pixels). The exposure time was adjusted to obtain baseline fluorescence intensity between 30-40 % of the CCD dynamic range. Fluorescence intensity changes in stratum radiatum near the site of LFP recording were averaged from 3 regions of interest >500µmmm distant from the stimulation

electrode tip using ImageJ software (NIH, USA). Data were expressed as the percentage changes in fluorescence over a baseline [(ΔF/F) • 100]. Signal analysis was performed using IgorPro software (WaveMetrics, Inc, OR, USA).

Tissue glucose and lactate concentrations were measured with enzymatic microelectrodes (tip diameter 25 µm; Sarissa Biomedical, Coventry, UK) polarized at 0.5V and driven with free radical analyzer TBR4100 (WPI, USA). Calibration was performed before and after each slice recording and the recorded data were corrected for eventual changes in electrode sensitivity. To avoid an interaction between enzymatic electrodes, glucose and lactate measurements were performed in separate sets of experiments.

Statistical analysis and signal processing. NAD(P)H dip and overshoot amplitudes as well as maximal changes in extracellular glucose/lactate concentrations were expressed as means ±SEM. Normality was rejected by Shapiro-Wilk normality test; and we used non-parametric Wilcoxon rank sum test. The level of significance was set at $p<0.05$.

Acknowledgments

This work was supported by Inserm, the European Union's Seventh Framework Programme (FP7/2007-2013) under grant agreement no602102 (EPITARGET) and ANR-14-CE13-0018-03. WL and SB are supported by the Niedersachsen-Research Network on Neuroinfectiology (N-RENNT) of the Ministry of Science and Culture of Lower Saxony in Germany. KJD and KL are supported by the Polish Ministry of Science and Higher Education grants 888/N-ESF-EuroEPINOMICS/10/2011/0 and W19/7.PR/2014.

Author contributions: AG, AMB GB and JAM performed experiments, and analyzed data. AB, AII, KJD, NG, SB, SJ, SS and WL performed experiments, analyzed data and wrote the manuscript. AB, KL, PB, MG and PSC supervised aspects of the project and wrote the manuscript. CB conceived and managed the project, performed experiments, analyzed data and wrote the manuscript.

Competing interests: all authors declare that they have no competing interests**.**

Data and materials availability: All the data is publicly available on the Circadiomics web portal at http://circadiomics.igb.uci.edu/.

Figures and Tables

A

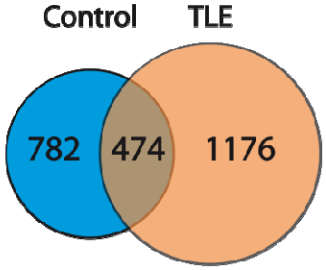

B

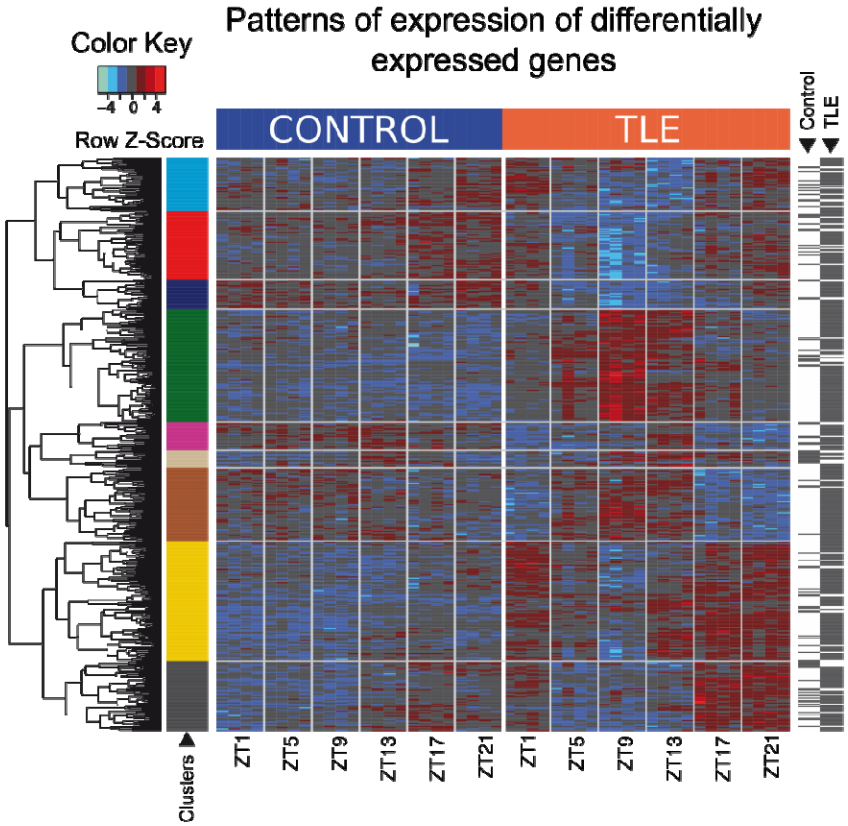

C

Functions of differentially expressed genes

	TERM	%	GENES
Cluster 1	phosphate metabolic process	16 %	MAST2, EIF2AK1, FLT1, ROCK2, ERBB3, WEE1, RNGTT
	protein phosphorylation	14 %	MAST2, EIF2AK1, FLT1, ROCK2, ERBB3, WEE1
	protein folding	7 %	GM6568, HSP90B1, AHSA1
Cluster 2	regulation of transcription	19 %	IRAK2, ZFP329, RBL2, HEXIM1, GABPA, ZFP760, HMG2 HDAC8, ZFP759, ZFP825
	chromosome organisation	10 %	RBL2, HMG20A, HSPA1B, ACIN1, HDAC8
	response to organic substance	8 %	PHIP, GLUL, DGCR8, STXBP4
Cluster3	cell cycle	17 %	CDC7, UHRF2, PRDM5, PLK1S1
Cluster4	transmembrane transport	7 %	SLC7A8, KCNA4, MFSD10, SLC25A16, SLC7A5, CACNA1
	regulation of cell proliferation	7 %	CEBPA, CAV2, FGFRL1, DBH, SOX9, F2R
Cluster5	proteolysis	23 %	EML2, QPCT, RAB40C, PSMA7, DNPEP
	circadian rhythm	9 %	DBP, PER3
Cluster6	rhythmic process	15 %	PER2, LFNG
Cluster7	translation	8 %	EIF6, MRPS15, LARS, DENR, VARS
	cellular homeostasis	7 %	GSR, TXNDC11, TFRC, SLC30A1
	behaviour	7 %	NPAS3, UBR3, CCL17, CYR61
Cluster8	oxidation reduction	7 %	XDH, DHRS3, FMO2, MAOB, AASS, ASPH, PRODH
	nucleosome assembly	4 %	HIST1H1E, H2AFV, HIST2H3C2, HIST2H4
Cluster9	chromosome organisation	11 %	2210018M11RIK, MSL1, HIST1H2BG, HSPA1A, BANP HIST1H3D

Potential regulators of differentially expressed genes

	TRANSCRIPTION FACTOR
Cluster 1	NF-Y
Cluster 4	Spz1, SMAD,PAX-4 LRF, Pax-8,ZF-5
Cluster 7	ZF5
Cluster 9	Zf5

Figure 1

Fig. 1. Circadian regulation of genes and proteins in the hippocampus and their reprogramming in epilepsy. (**A**) Transcripts oscillating in circadian rhythm. In control mice (n=4 per Zeitgeber Time – ZT), 1256 transcripts are oscillating. In TLE (n=4 per ZT), more transcripts are oscillating (1650). Only 474 are common to both conditions, showing a remodeling of the landscape of oscillating genes in TLE. (**B**) Heatmap of 486 mRNAs showing circadian differential expression. 67 mRNAs were differentially expressed in at least one time point only in control animals, 384 mRNAs were differentially expressed only in TLE and 35 mRNAs were differentially expressed in both groups. Each column per time window represents an individual animal and each row represents an individual mRNA. Colors on the heatmap represent Z-score: higher – red, lower – blue. The hour of tissue collection is indicated below (ZT). The dendrogram obtained from hierarchical clustering is shown on the left side of the heatmap panel. Genes are ordered by clustering complete-linkage method together with Pearson correlation distance measure. Colors in the bar on the left side of the heatmap panel represent clusters obtained by cutting dendrogram at selected level heights to obtain nine groups. Black lines in the bar on the right side of the heatmap panel mark genes showing differences in expression between control or TLE animals based on one-way ANOVA – analysis of variance (cut-off FDR < 0.05)

(**C**) Left panel: biological functions for each gene cluster (defined on the heatmap from panel (**A**)) according to Gene Ontology vocabulary using DAVID. Only terms, which are represented by more than 5% of genes in a given cluster, are presented in the Table. Right bottom panel: Transcription factors with binding sites overrepresented in different gene clusters defined on the heatmap from panel (**B**).

A

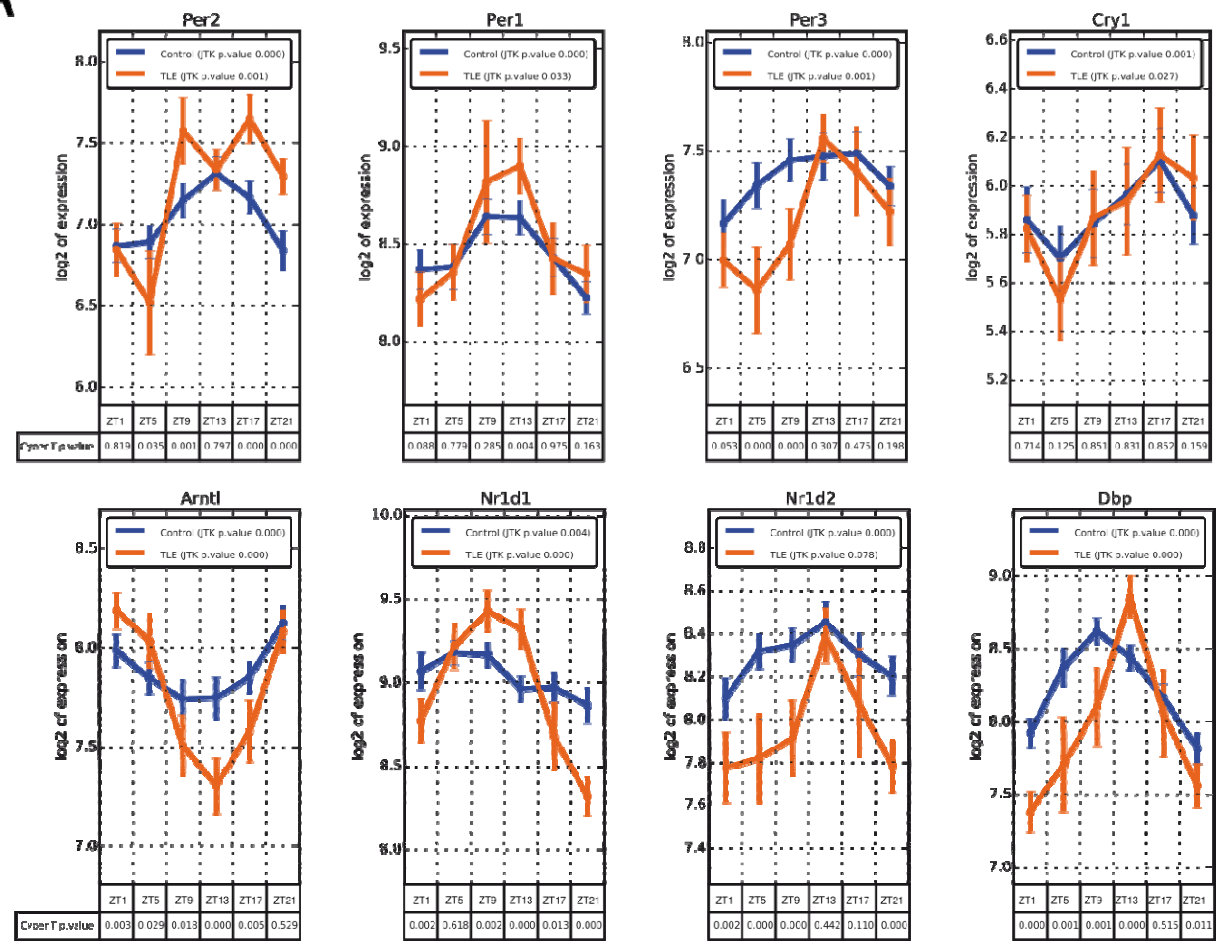

B

Gene	Control Amp	Epileptic Amp
Bhlhe40	0.2375081574	0.4140875868
Bhlhe41	0.3839730036	0.8064160334
Arntl	0.3834664913	0.8833480509
Hdac8	0.1094111846	0.4769890427
Runx1	0.1811503567	0.7019302037
Per2	0.4750034544	1.130855182
Cry1	0.4035340666	0.5957495958

Figure 2

Fig. 2. Oscillation patterns and amplitudes of core clock genes. Note the phase change and general increase in oscillation amplitude in TLE as compared to controls.

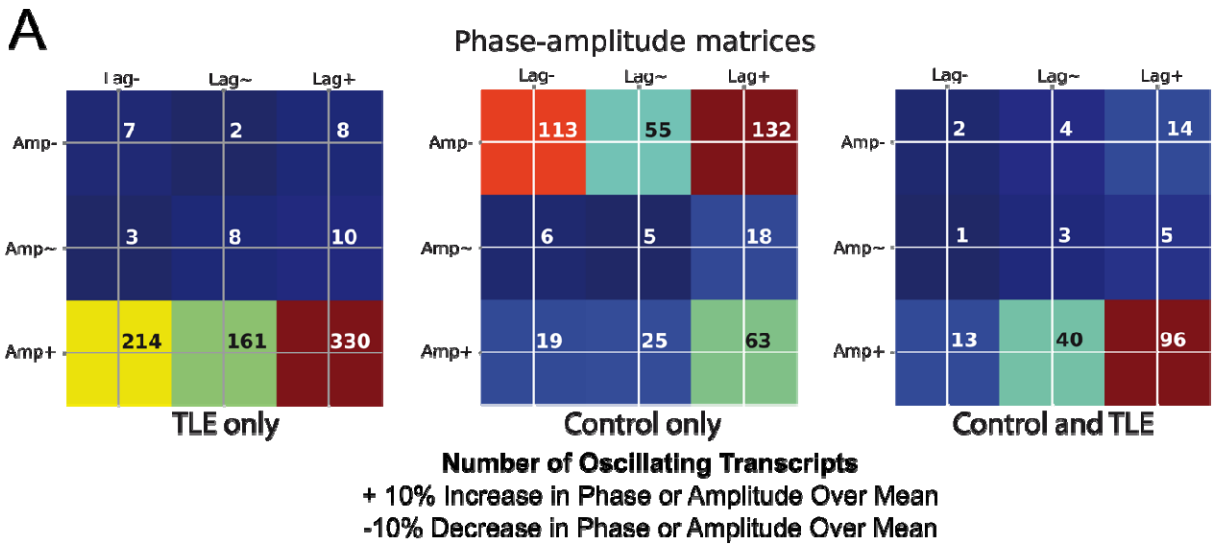

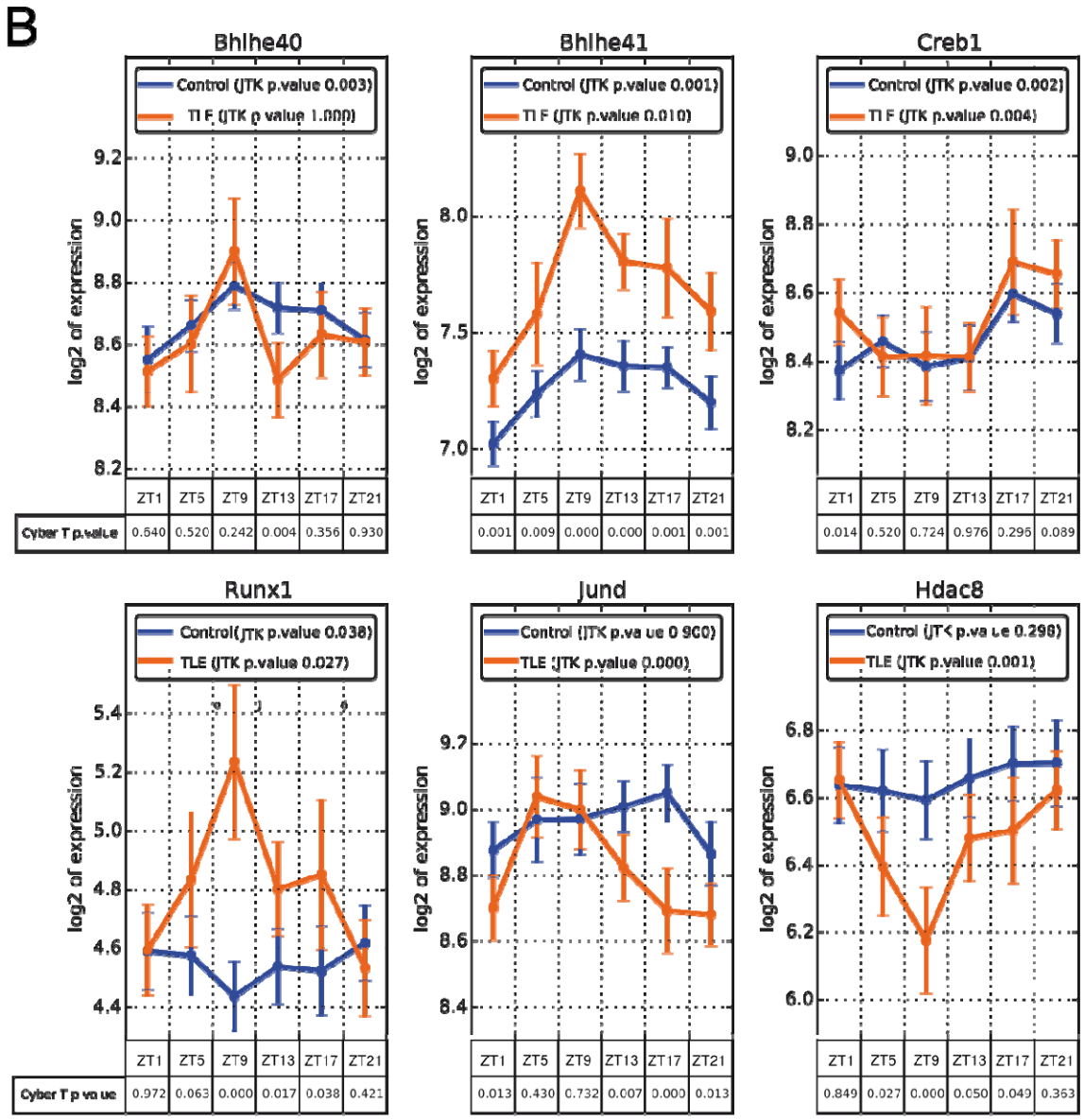

Figure 3

Fig. 3. Different oscillatory patterns of gene transcripts in control mice and their alterations in TLE. (**A**) Phase-Amplitude matrices. Most of the transcripts show high amplitude oscillations in TLE, whilst they are distributed in controls between low and high amplitude. The majority of high amplitude oscillatory transcripts are phase advanced as compared to the rest of the oscillatory transcripts, a property more pronounced in TLE. The number of oscillating transcripts is labelled in each box. Boxes are defined as phase delayed "Lag -", phase advanced "Lag +", or no phase change in the columns. Rows indicate the amplitude. Advanced or delayed amplitude or phase is taken as a minimum 10% change over the total mean for amplitude and phase, receptively. The number of oscillating transcripts is color-coded. Blue indicates the lowest values and dark red indicates the highest values per condition (Control-Alone, TLE-Alone, Both). (**B**) Oscillatory patterns of genes, which may contribute to the reprogramming of the circadian hippocampal remapping in TLE. *Creb1* oscillates in both conditions. Key controllers of circadian rhythms, *Bhlhe40* and *Bhlhe41*, show increased oscillation amplitudes in TLE, which may contribute to the large recruitment of oscillating genes in TLE. *Runx1*, a DNA binding regulator, and *Hdac8*, a chromatin remodeler, gain statistically significant oscillation in TLE. *JunD* (which interacts with both the AP-1 transcription factor complex and *Creb1*) shows a 180° phase shift in TLE as compared to control.

Legend for the Figure: **A.** Heatmap presenting the difference between control and TLE animals in selected gene set activity (cut-off p-value < 0.05); changes in gene sets activity were in range from 0.8677739 to 1.2963374. Values presented on the heatmap are FDR based significance score calculated as follows: -log10(p-value) * sign(log(fold change)). **B** the comparison of metabolic signals recorded in hippocampal slices prepared at ZT3 and ZT8 from TLE (yellow or red traces) and control (gray or black) brains. The results of statistical analysis (nonparametric Wilcoxon-Mann-Whitney test) are provided in the main text.

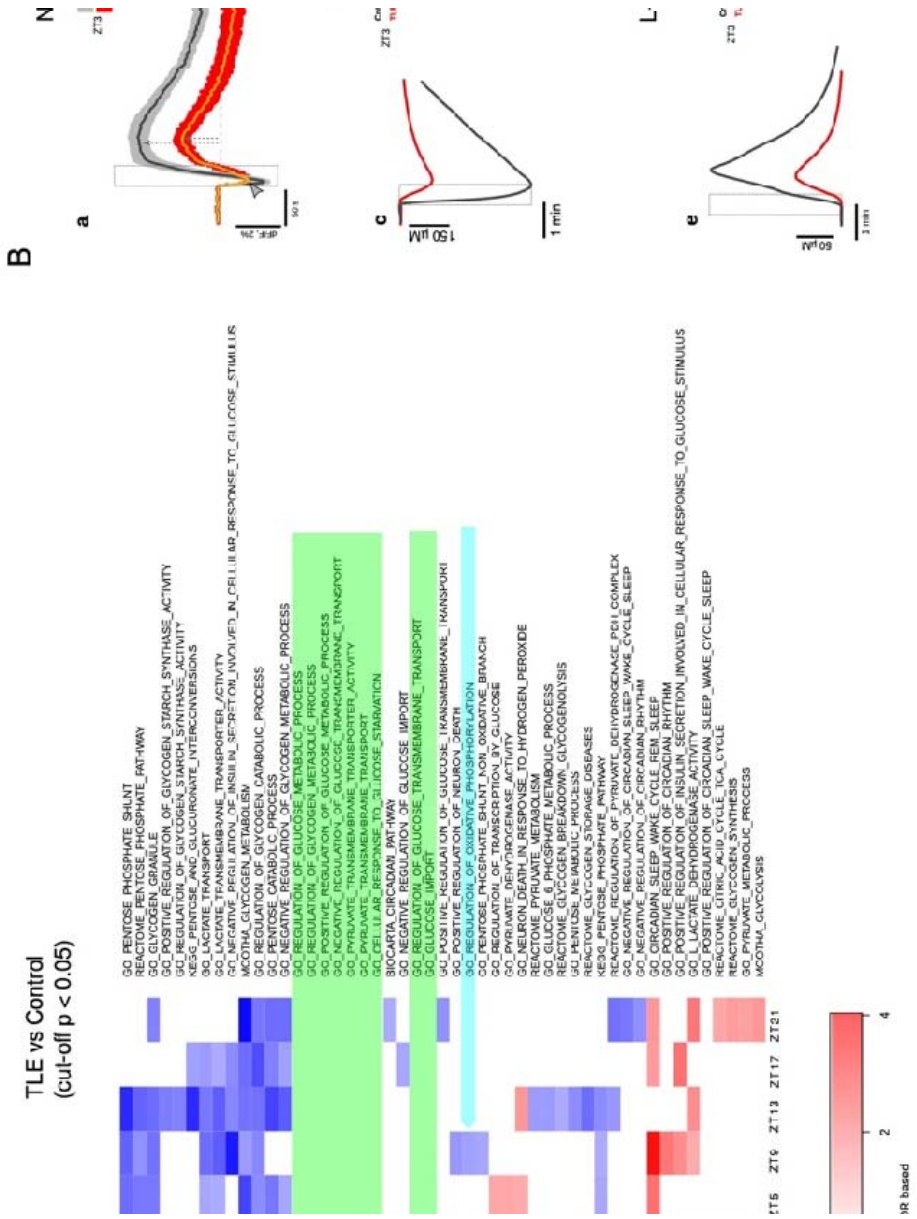

Figure 4

Fig. 4. Alteration of circadian regulation of energy metabolism in TLE.

(A) Heatmap presenting the difference between control and TLE animals in selected gene set activity (cut-off p-value < 0.05). Changes in gene sets activity were in the range from 0.87 to 1.30. Values presented on the heatmap are FDR based significance score calculated as follows: -log10(p-value) * sign(log(fold change)). Light green emphasizes gene sets involved in glucose aerobic metabolism. Light blue shows a gene set associated with oxidative metabolism. **(B)** Metabolic activity induced by 10 Hz 30s electrical pulse train stimulation of Schafer collaterals (dashed rectangle) evaluated using NAD(P)H imaging (a, b), glucose (c, d), and lactate (e, f) sensing in Stratum Radiatum of hippocampal slices of control and TLE mice. (a) Averaged

NAD(P)H fluorescence recorded in TLE (yellow trace) and control (dark gray trace) slices prepared at ZT3. The mean amplitude of the NAD(P)H transient overshoot was significantly smaller in TLE than in control mice (TLE: 1.3±0.17% n=9, control: 3.5±0.5%, n=10, $p<0.01$, dashed arrows) suggesting reduced activity of cytosolic glycolysis in TLE as compared to control. (b) There was no difference in NAD(P)H overshoot in slices prepared at ZT8 in TLE (red trace) and control (grey trace) mice (TLE: 4.1±0.4%, n=6, control: 4.6±0.9%, n=6, p=0.3). However, dip amplitudes (grey arrow heads) were significantly smaller in TLE than in control (-0.6±0.1%, vs -1.7±0.3%, $p<0.05$) indicating a reduced activity of oxidative phosphorylation. Glucose consumption (c) and lactate release (e) induced by synaptic stimulation were lower in TLE (red traces) when the slices were cut at ZT3 (glucose: 0.13±0.03 mM vs 0.52± 0.14 mM, $p<0.01$, n=9; lactate: 0.04±0.01 mM vs 0.19±0.05 mM, $p<0.01$, n=7). In the afternoon (ZT8), both parameters were increased in TLE slices (glucose: 0.41±0.08 mM ; lactate: 0.12±0.01 mM, n=6) indicating enhanced aerobic glycolysis activity (d, f red traces). In control slices, glucose consumption (d, grey trace) increased with time (1.00±0.4 mM n=5) while lactate release profile (f vs e, grey traces) had a lower amplitude as compared to ZT3 (0.11 ± 0.01mM, n=6) and displayed a short lasting lactate decrease at the beginning of the stimulation (f, grey arrow head).

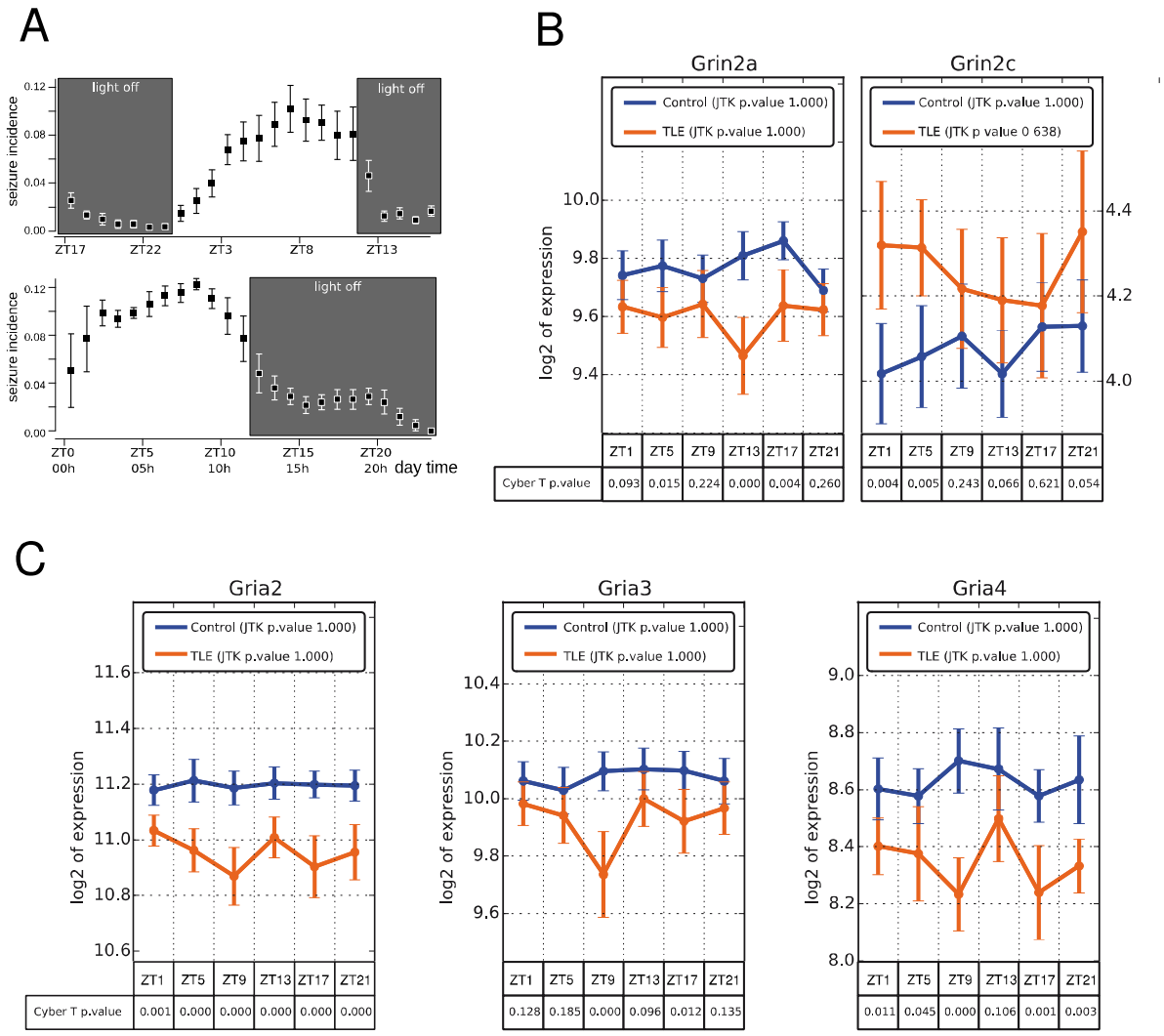

Figure 5

Fig. 5. Circadian regulation of seizures and drug targets in TLE.

(**A**) Top. Circadian regulation of seizure incidence during the night and day cycle. The highest seizure probability is found around ZT8. Bottom. Two days after shifting the light/dark cycle by 8 hours in the animal facility, the temporal pattern of seizure incidence shifted accordingly. (**B** and **C**) Alterations of the temporal expression of genes encoding for NMDA and AMPA receptors subunits, respectively.

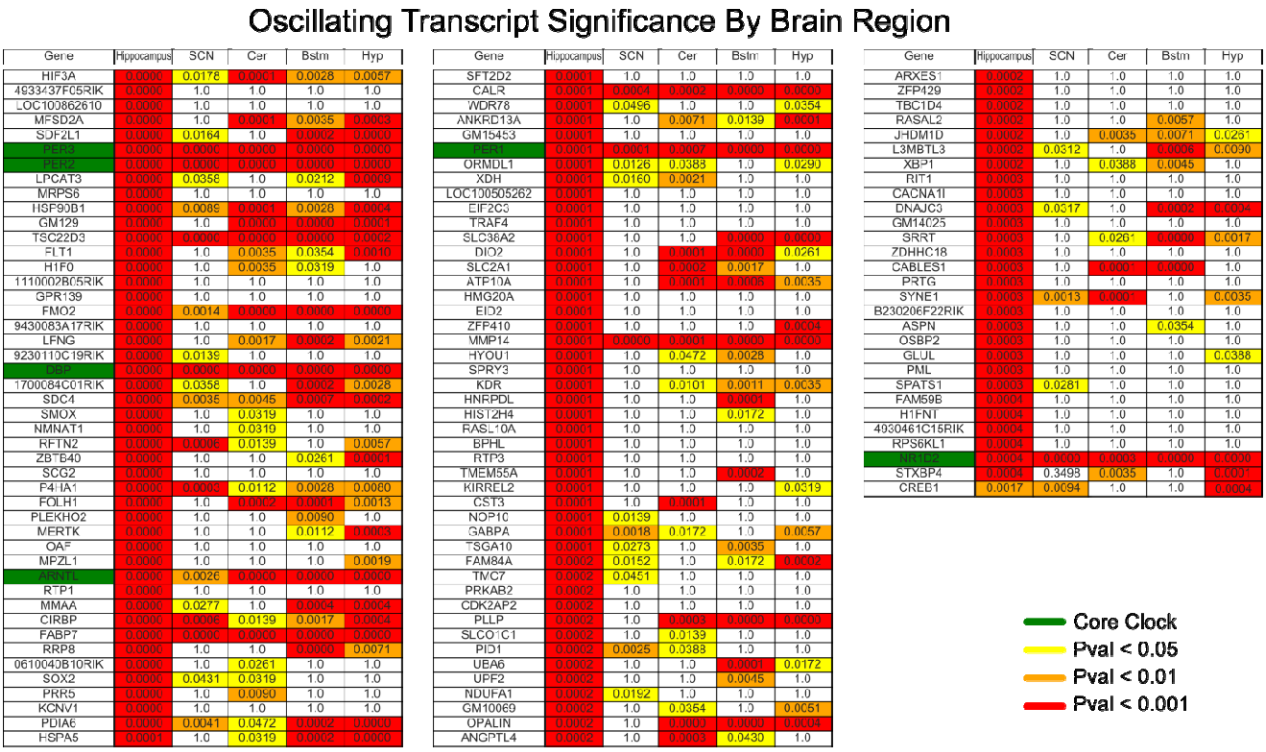

Table 1

Table 1. List of genes showing a circadian regulation in control mice, in the hippocampus (Hippocampus), suprachiasmatic nucleus (SCN), Cerebellum (Cer), Brain Stem (Bstm) and Hypothalamus (Hyp). If most core clock genes display circadian regulation in most structures, numerous genes oscillate specifically in the hippocampus.

Type of action	Oscillating genes Control	Oscillating genes TLE	Expression change Control	Expression change TLE
Target	ADAM10, BPHL, **CACNA1I**, CALR, CRBN, FLT1, FOLH1, GLUL, HSP90B1, HSPA5, IGF1R, KDR, MERTK, MMAA, MMP14, NDUFA1, NDUFA6, NMNAT1, NPEPPS, P4HA1, PRKAB2, RAB8B, SMOX, XDH	***ABCC1***, ACAN, ADRBK1, ADSSL1, AFG3L2, AKT2, ALAS1, ALDH6A1, ALKBH3, ANO1, APRT, BCL2, CD52, CTSK, CYB5R3, CYSLTR2, DDAH2, DHPS, DNPEP, EDNRB, F2R, FASN, FPGS, GARS, GLS, GLUL, GPT2, GRIK5, GRM7, GSR, HCN2, HDAC6, HDAC8, HIF1AN, HRH3, IMPG2, LARS, MAPT, MERTK, MLLT4, MMAA, MMP14, MTRR, NDUFA10, NFKBIA, PDE7A, PFN1, PIK3CA, PRKAB1, PSMA4, PSMA7, PSMB7, PTPRS, QPCT, RAB8B, RNGTT, RPL19, RPS6KA4, RYR2, SGPL1, SHMT1, SLC15A2, SLC16A3, SLC6A9, SLC7A8, STMN4, SULT2B1, TSTA3, TUBD1, VARS, WEE1	ADAM10, BRAF, CALR, CXCR4, FLT1, FOLH1, GLUL, HSP90B1, HSPA5, MERTK, MMAA, NDUFA1, NDUFA6, NFKBIA, P4HA1, PRKAB2, SLC16A1, SMOX, TOP1, XDH	AASS, ***ABCC1***, ADSSL1, AGT, AKT2, ALDH6A1, ALDH7A1, AMT, APRT, ASPH, CACNA1B, CALR, CD44, CYB5R3, CYSLTR2, DBH, DDAH2, DDX6, DHPS, DHRS3, DNPEP, F2R, **GABRA3**, GLUL, GPT2, GSR, GSTM5, HDAC6, HDAC8, HIF1AN, HSP90B1, HSPA5, HSPB1, IMPG2, KCNA4, LARS, **MAOB**, MERTK, MLLT4, MMAA, NCOA5, NDUFA10, NFKBIA, P4HA1, PAICS, PDE7A, PDK4, PRKAB1, PRODH, PSMA7, PTPRS, QPCT, RB1, RNGTT, ROCK2, SERPINF2, SHMT1, SLC7A8, SULT2B1, TUBD1, VARS, WEE1
Carrier	FABP7, SLC2A1	FABP5, SLC2A1	FABP7, SLC2A1	
Enzyme	GLUG, XDH	APRT, FPGS, GLS, GLUL, GSR, HIF1AN, VARS	GLUL, XDH	APRT, CHKA, DBH, GLUL, GSR, HIF1AN, MAOB, PRODH, SRM, TGM1, VARS
Transporter	SLC2A1, **SLCO1C1**	**ABCC1**, ABCC5, SLC15A2, SLC16A3, SLC2A1, SLC2A9, SLC7A5, SLC7A8, TFRC	**SLC16A1**, SLC2A1	**ABCC1**, ABCC5, SLC14A1, SLC2A9, SLC7A5, SLC7A8, TFRC

Table 2

Table 2. List of genes that oscillate (JTK_CYCLE adjusted p < 0.05) or are differentially expressed during circadian cycle (one-way ANOVA, FDR < 0.05) in control animals and/or experimental TLE. Genes are separated in drug targets, carriers, enzymes and transporters. There is little overlap between the control and TLE conditions (common ones are underlined). The ABCC1 is not only transporter for Phenobarbital but also a drug target for Sulfinpyrazone and Biricodar dicitrate (in italics). Genes in Bold are shown in Table3.

Gene symbol	Function	OSC	DE	Animals	Anticonvulsant Drug names
ABCC1	Tr	+	+	TLE	Phenobarbital
CACNA1B	T	-	+	TLE	Gabapentin, Levetiracetam
CACNA1I	T	+	-	CTR	Paramethadione, Zonisamide and Flunarizine
GABRA3	T	-	+	TLE	Meprobamate, Metharbital, Thiopental, Primidone, Diazepam, Methylphenobarbital, Estazolam, Fludiazepam, Nitrazepam
MAOB	T	-	+	TLE	Zonisamide
SLC16A1	Tr	-	+	CTR	Valproic Acid
SLCO1C1	Tr	+	-	CTR	Phenytoin

Table 3. Genes that are drug target (T) or transporters (Tr), and that oscillate (JTK_CYCLE, adjusted p value < 0.05; OSC) or that are differentially expressed (one-way-ANOVA, adjusted p value < 0.05; DE) in control (CTR) or TLE animals. Information on drugs can be found in the Supplementary Materials.

References

1. S. Masri, P. Sassone-Corsi, The circadian clock: a framework linking metabolism, epigenetics and neuronal function. *Nat Rev Neurosci* **14**, 69-75 (2013).
2. K. Eckel-Mahan, P. Sassone-Corsi, Metabolism and the circadian clock converge. *Physiol Rev* **93**, 107-135 (2013).
3. C. Guilding, H. D. Piggins, Challenging the omnipotence of the suprachiasmatic timekeeper: are circadian oscillators present throughout the mammalian brain? *Eur J Neurosci* **25**, 3195-3216 (2007).
4. V. L. Harbour, Y. Weigl, B. Robinson, S. Amir, Comprehensive mapping of regional expression of the clock protein PERIOD2 in rat forebrain across the 24-h day. *PLoS One* **8**, e76391 (2013).
5. L. E. Chun, E. R. Woodruff, S. Morton, L. R. Hinds, R. L. Spencer, Variations in Phase and Amplitude of Rhythmic Clock Gene Expression across Prefrontal Cortex, Hippocampus, Amygdala, and Hypothalamic Paraventricular and Suprachiasmatic Nuclei of Male and Female Rats. *J Biol Rhythms* **30**, 417-436 (2015).
6. S. Yang, K. Wang, O. Valladares, S. Hannenhalli, M. Bucan, Genome-wide expression profiling and bioinformatics analysis of diurnally regulated genes in the mouse prefrontal cortex. *Genome Biol* **8**, R247 (2007).
7. J. Z. Li *et al.*, Circadian patterns of gene expression in the human brain and disruption in major depressive disorder. *Proc Natl Acad Sci U S A* **110**, 9950-9955 (2013).
8. F. Bruning *et al.*, Sleep-wake cycles drive daily dynamics of synaptic phosphorylation. *Science* **366**, (2019).
9. S. B. Noya *et al.*, The forebrain synaptic transcriptome is organized by clocks but its proteome is driven by sleep. *Science* **366**, (2019).
10. B. J. Shannon *et al.*, Morning-evening variation in human brain metabolism and memory circuits. *J Neurophysiol* **109**, 1444-1456 (2013).
11. J. R. Gerstner *et al.*, Cycling behavior and memory formation. *J Neurosci* **29**, 12824-12830 (2009).
12. S. Sahar, P. Sassone-Corsi, Circadian rhythms and memory formation: regulation by chromatin remodeling. *Frontiers in molecular neuroscience* **5**, 37 (2012).
13. B. L. Smarr, K. J. Jennings, J. R. Driscoll, L. J. Kriegsfeld, A time to remember: the role of circadian clocks in learning and memory. *Behav Neurosci* **128**, 283-303 (2014).
14. C. A. Barnes, B. L. McNaughton, G. V. Goddard, R. M. Douglas, R. Adamec, Circadian rhythm of synaptic excitability in rat and monkey central nervous system. *Science* **197**, 91-92 (1977).
15. K. M. Harris, T. J. Teyler, Age differences in a circadian influence on hippocampal LTP. *Brain Res* **261**, 69-73 (1983).
16. D. Chaudhury, L. M. Wang, C. S. Colwell, Circadian regulation of hippocampal long-term potentiation. *J Biol Rhythms* **20**, 225-236 (2005).
17. K. L. Eckel-Mahan *et al.*, Circadian oscillation of hippocampal MAPK activity and cAmp: implications for memory persistence. *Nat Neurosci* **11**, 1074-1082 (2008).
18. K. L. Eckel-Mahan *et al.*, Reprogramming of the circadian clock by nutritional challenge. *Cell* **155**, 1464-1478 (2013).
19. F. Gachon, U. Loizides-Mangold, V. Petrenko, C. Dibner, Glucose Homeostasis: Regulation by Peripheral Circadian Clocks in Rodents and Humans. *Endocrinology* **158**, 1074-1084 (2017).
20. C. M. Greco, P. Sassone-Corsi, Circadian blueprint of metabolic pathways in the brain. *Nat Rev Neurosci* **20**, 71-82 (2019).
21. J. S. Duncan, G. P. Winston, M. J. Koepp, S. Ourselin, Brain imaging in the assessment for epilepsy surgery. *Lancet Neurol* **15**, 420-433 (2016).
22. M. M. Verbeek, W. G. Leen, M. A. Willemsen, D. Slats, J. A. Claassen, Hourly analysis of cerebrospinal fluid glucose shows large diurnal fluctuations. *J Cereb Blood Flow Metab* **36**, 899-902 (2016).
23. O. Al-Iedani *et al.*, Diurnal stability and long-term repeatability of neurometabolites using single voxel 1H magnetic resonance spectroscopy. *Eur J Radiol* **108**, 107-113 (2018).
24. J. Arm, O. Al-Iedani, R. Lea, J. Lechner-Scott, S. Ramadan, Diurnal variability of cerebral metabolites in healthy human brain with 2D localized correlation spectroscopy (2D L-COSY). *J Magn Reson Imaging* **50**, 592-601 (2019).
25. D. J. Buysse *et al.*, Regional brain glucose metabolism during morning and evening wakefulness in humans: preliminary findings. *Sleep* **27**, 1245-1254 (2004).
26. E. J. Bartlett *et al.*, Reproducibility of cerebral glucose metabolic measurements in resting human subjects. *J Cereb Blood Flow Metab* **8**, 502-512 (1988).
27. A. Germain *et al.*, Diurnal variation in regional brain glucose metabolism in depression. *Biol Psychiatry* **62**, 438-445 (2007).
28. R. Silver, L. J. Kriegsfeld, Circadian rhythms have broad implications for understanding brain and behavior. *Eur J Neurosci* **39**, 1866-1880 (2014).
29. R. Zhang, N. F. Lahens, H. I. Ballance, M. E. Hughes, J. B. Hogenesch, A circadian gene expression atlas in mammals: implications for biology and medicine. *Proc Natl Acad Sci U S A* **111**, 16219-16224 (2014).

30. M. E. Hughes, J. B. Hogenesch, K. Kornacker, JTK_CYCLE: an efficient nonparametric algorithm for detecting rhythmic components in genome-scale data sets. *J Biol Rhythms* **25**, 372-380 (2010).
31. L. S. Mure *et al.*, Diurnal transcriptome atlas of a primate across major neural and peripheral tissues. *Science* **359**, (2018).
32. K. Daily, V. R. Patel, P. Rigor, X. Xie, P. Baldi, MotifMap: integrative genome-wide maps of regulatory motif sites for model species. *BMC Bioinformatics* **12**, 495 (2011).
33. B. Bode, R. Taneja, M. J. Rossner, H. Oster, Advanced light-entrained activity onsets and restored free-running suprachiasmatic nucleus circadian rhythms in per2/dec mutant mice. *Chronobiol Int* **28**, 737-750 (2011).
34. F. Lu, Q. Liu, Validation of RUNX1 as a potential target for treating circadian clock-induced obesity through preventing migration of group 3 innate lymphoid cells into intestine. *Med Hypotheses* **113**, 98-101 (2018).
35. M. E. Reale *et al.*, The transcription factor Runx2 is under circadian control in the suprachiasmatic nucleus and functions in the control of rhythmic behavior. *PLoS One* **8**, e54317 (2013).
36. M. S. Robles, J. Cox, M. Mann, In-vivo quantitative proteomics reveals a key contribution of post-transcriptional mechanisms to the circadian regulation of liver metabolism. *PLoS Genet* **10**, e1004047 (2014).
37. F. Chassoux *et al.*, Determinants of brain metabolism changes in mesial temporal lobe epilepsy. *Epilepsia* **57**, 907-919 (2016).
38. T. S. McDonald, C. Carrasco-Pozo, M. P. Hodson, K. Borges, Alterations in Cytosolic and Mitochondrial [U-(13)C]Glucose Metabolism in a Chronic Epilepsy Mouse Model. *eNeuro* **4**, (2017).
39. S. Vielhaber *et al.*, Correlation of hippocampal glucose oxidation capacity and interictal FDG-PET in temporal lobe epilepsy. *Epilepsia* **44**, 193-199 (2003).
40. D. E. Kuhl, J. Engel, Jr., M. E. Phelps, C. Selin, Epileptic patterns of local cerebral metabolism and perfusion in humans determined by emission computed tomography of 18FDG and 13NH3. *Ann Neurol* **8**, 348-360 (1980).
41. C. Dube, S. Boyet, C. Marescaux, A. Nehlig, Relationship between neuronal loss and interictal glucose metabolism during the chronic phase of the lithium-pilocarpine model of epilepsy in the immature and adult rat. *Exp Neurol* **167**, 227-241 (2001).
42. G. Yaari, C. R. Bolen, J. Thakar, S. H. Kleinstein, Quantitative set analysis for gene expression: a method to quantify gene set differential expression including gene-gene correlations. *Nucleic Acids Res* **41**, e170 (2013).
43. A. Liberzon *et al.*, Molecular signatures database (MSigDB) 3.0. *Bioinformatics* **27**, 1739-1740 (2011).
44. A. Subramanian *et al.*, Gene set enrichment analysis: a knowledge-based approach for interpreting genome-wide expression profiles. *Proc Natl Acad Sci U S A* **102**, 15545-15550 (2005).
45. A. I. Ivanov, C. Bernard, D. A. Turner, Metabolic responses differentiate between interictal, ictal and persistent epileptiform activity in intact, immature hippocampus in vitro. *Neurobiol Dis* **75**, 1-14 (2015).
46. M. Quigg, M. Straume, M. Menaker, E. H. Bertram, 3rd, Temporal distribution of partial seizures: comparison of an animal model with human partial epilepsy. *Ann Neurol* **43**, 748-755 (1998).
47. V. K. Jirsa, W. C. Stacey, P. P. Quilichini, A. I. Ivanov, C. Bernard, On the nature of seizure dynamics. *Brain* **137**, 2210-2230 (2014).
48. V. Law *et al.*, DrugBank 4.0: shedding new light on drug metabolism. *Nucleic Acids Res* **42**, D1091-1097 (2014).
49. M. A. Rogawski, W. Loscher, J. M. Rho, Mechanisms of Action of Antiseizure Drugs and the Ketogenic Diet. *Cold Spring Harb Perspect Med* **6**, (2016).
50. R. G. Munn, D. K. Bilkey, The firing rate of hippocampal CA1 place cells is modulated with a circadian period. *Hippocampus* **22**, 1325-1337 (2012).
51. R. G. Munn, S. M. Tyree, N. McNaughton, D. K. Bilkey, The frequency of hippocampal theta rhythm is modulated on a circadian period and is entrained by food availability. *Front Behav Neurosci* **9**, 61 (2015).
52. J. Q. M. Ly *et al.*, Circadian regulation of human cortical excitability. *Nat Commun* **7**, 11828 (2016).
53. L. M. Wang *et al.*, Expression of the circadian clock gene Period2 in the hippocampus: possible implications for synaptic plasticity and learned behaviour. *ASN Neuro* **1**, (2009).
54. V. L. Harbour, Y. Weigl, B. Robinson, S. Amir, Phase differences in expression of circadian clock genes in the central nucleus of the amygdala, dentate gyrus, and suprachiasmatic nucleus in the rat. *PLoS One* **9**, e103309 (2014).
55. C. L. Thompson *et al.*, Genomic anatomy of the hippocampus. *Neuron* **60**, 1010-1021 (2008).
56. L. M. Prolo, J. S. Takahashi, E. D. Herzog, Circadian rhythm generation and entrainment in astrocytes. *J Neurosci* **25**, 404-408 (2005).
57. S. McClelland *et al.*, The transcription factor NRSF contributes to epileptogenesis by selective repression of a subset of target genes. *Elife* **3**, e01267 (2014).
58. K. Kobow, I. Blumcke, Epigenetic mechanisms in epilepsy. *Prog Brain Res* **213**, 279-316 (2014).

59. H. Manouze *et al.*, Effects of Single Cage Housing on Stress, Cognitive, and Seizure Parameters in the Rat and Mouse Pilocarpine Models of Epilepsy. *eNeuro* **6**, (2019).
60. E. S. Musiek, D. M. Holtzman, Mechanisms linking circadian clocks, sleep, and neurodegeneration. *Science* **354**, 1004-1008 (2016).